In-process defect characterization method for nanostructured surfaces

A. Tausendfreund[1,#], M. Zimmermann[1],M. Z. Shaikh[2],S. Kieß[2], S. Patzelt[1], S. Simon[2]and G. Goch[1]

1 Bremen Institute for Metrology, Automation and Quality Science (BIMAQ),28359 Bremen, Linzer Straße 13, Germany
2 Institute of Parallel and Distributed Systems (IPVS), 70569 Stuttgart,Universitätsstraße 38, Germany
tau@bimaq.de, TEL: +49 (0)421-218-646 41, FAX: +49 (0)421-218-646 70

KEYWORDS :In-process and on-line measurement, Micro/nano- metrology, Light Scattering, Far-Field Simulation

Laser light scattering measurements offer a high potential for in-process applications in mass production because they provide surface data quickly, integrally and contact-free. From a measured light scattering distribution of a nanostructured surface one cannot infer directly to the underlying topography. Therefore the idea of an in-process measurement procedure for nanostructured surfaces bases on a comparison between a multitude of simulated and measured speckle patterns. This paper applies a hardware accelerated rigorous simulation method, which enables calculating light scattering from nanostructured surfaces in reasonable computation times. These simulations are verified by a measurement setup, which detects angle resolved scattered light. For a first application in the field of quality control the results of the comparison are evaluated. Indeedfor zinc oxide nanograss structures it is shown that by measuring the scattered light distribution it is possible to distinguish between defect-free and defective nanostructures.

Manuscript received: JanuaryXX, 2011 / Accepted: JanuaryXX, 2011

1. Introduction

Microtechnology and nanotechnology are emerging as a driving force for economic growth and development in the 21st century. The potential nanotechnology related markets around the world have been forecast to reach $1 trillion by 2015. These predictions result in an increased need for measuring systems in the future, to be able to characterize nanostructures close to the process or during a running production process. In the production phase, the quantitative evaluation of individual structures is less significant, as compared to a fast and extensive qualitative assessment of the structures and their functionality. Deviations from a required production result generally do not appear randomly, but can be classified according to the production process into typical defect classes. Examples from the large number of applications are nanograss structured surfaces.

Nanograss structures facilitate the growth of organic cells on technical surfaces, the targeted transfer of heat from the silicon chip to the cooling medium or the creation of dirt-resistant surface coatings. The nanograss structures shown in Fig. 1a are useable in the future for LED based large area displays. Defect classes are here e.g. a low dipole density accompanied by ranges without rods and statistically bended rods (Fig.1b). Areas with missing ZnO nano-rods can result in short circuits between the top anode and the bottom cathode electrodes.An optical measurement system, offering the possibility to distinguish between the defect classes and to characterize these in a running production process, would be of great economic interest.

Optical measurements based on laser light scattering provide surface data fast, integrally and contact-free. The information about the nanostructured surface topography is contained within the scattered light distribution, hence they are particularly suited for rapidly recognizing defects [1, 2]. Subsequently they offer a high potential for in-process applications in mass production.

Fundamentally, a measured light scattering distribution cannot be traced back directly to the underlying topography.Furthermore, the light scattering effects that arise from the surface defects cannotalways be recognized immediately as such.

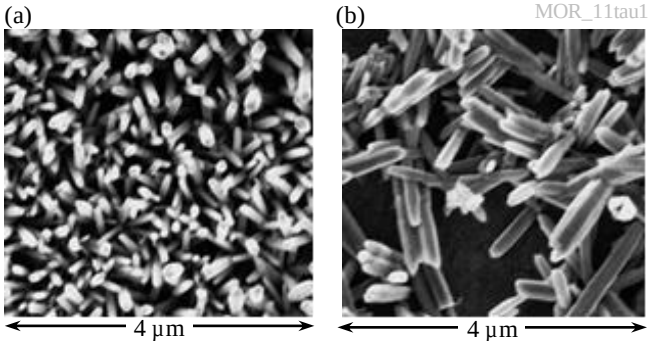

Figure 1. Examples of nanograss structured surfaces (a) defect-free nanograss structure; (b) defective nanograss structure (source: Institute of Solid State Physics, Bremen University, Germany).

The idea of an in-process measurement system for microstructured and nanostructured surfaces therefore is based on thecomparison of the simulated and the measured scattered light pattern.The important aspect here is not just the fundamental knowledge about the scattered light distribution of the desired nanostructure, but also a comprehensive understanding of how the defective structures affect the light scattering pattern. If, by means of a reasonable number of simulations, it is possible to calculate light scattering distributions for one class of typical defects (e.g. the statistically bended nano-rods of Fig. 1b), then the measurement system combined with a neural network can be statistically trained to recognize these defects quickly. This might also detect the deviations in a running production process.

As the classical scalar diffraction theory fails for surface structures with curvature radii in the sub-wavelength range [3], itis currently not possible to calculate the light scattering distribution of nanostructured surfaces for technically reasonable lateral measuring areas. Therefore, new and fast rigorous light scattering simulation algorithms are needed. A procedure that is suitable for hardware acceleration on a computer graphic card is called discrete dipole approximation (DDA) [4] and is described in the following.

2. Simulation of Light Scattering Experiments

2.1 Discrete Dipole Approximation (DDA)

The method of discrete dipole approximation uses an approximation of an arbitrarily shaped particle by an agglomerate of N individual point dipoles. The important fact is that for infinitesimal distances between these dipoles the DDA-approach turns into the exact integral form of Maxwell's equations on the light scattering problem [5].

Each individual dipole at the point $\boldsymbol{r}_j$of the scattering body possesses an oscillating polarization$\boldsymbol{P}_j$that depends on the incident field

$$\boldsymbol{E}_{inc,j} = \boldsymbol{E}_0 \exp\left(i\boldsymbol{k}\cdot\boldsymbol{r}_j - i\omega t\right) \tag{1}$$

and on the field $\boldsymbol{E}_{other,j}$, which is defined by the interaction of the dipoles among themselves:

$$\boldsymbol{P}_j = \alpha_j\left(\boldsymbol{E}_{inc,j} + \boldsymbol{E}_{other,j}\right) = \alpha_j\left(\boldsymbol{E}_{inc,j} - \sum_{k\neq j}^{N} A_{jk}\boldsymbol{P}_k\right). \tag{2}$$

$\boldsymbol{E}_0$ is the amplitude of the incident field, $\boldsymbol{k}$ the wave vector, ω the angular frequency and $A_{jk}\boldsymbol{P}_k$the electric field at the point $\boldsymbol{r}_j$, caused by the dipole $\boldsymbol{P}_k$at the position$\boldsymbol{r}_k$. The polarizability α_j at the position $\boldsymbol{r}_j$and the matrix element A_{jk} are in general 3 x 3 tensors. The product$A_{jk}\boldsymbol{P}_k$ is described by:

$$A_{jk}\boldsymbol{P}_k = \frac{\exp(ikr_{jk})}{r_{jk}^3}\left\{k^2\boldsymbol{r}_{jk}\times(\boldsymbol{r}_{jk}\times\boldsymbol{P}_k) + \frac{(1-ikr_{jk})}{r_{jk}}\left[r_{jk}^2\boldsymbol{P}_k - 3\boldsymbol{r}_{jk}(\boldsymbol{r}_{jk}\boldsymbol{P}_k)\right]\right\}. \tag{3}$$

The vector $\boldsymbol{r}_{jk}$ represents the difference between $\boldsymbol{r}_j$and $\boldsymbol{r}_k$, accordingly itsabsolute value is defined by $r_{jk} = |\boldsymbol{r}_j - \boldsymbol{r}_k|$. For isotropic media, the polarizability α_j is a scalar. The simplest method to approximate the polarizability is given by the Clausius-Mosotti equation:

$$\alpha_j^{CM} = 3d^3\varepsilon_0\frac{\varepsilon_j - \varepsilon_0}{\varepsilon_j + 2\varepsilon_0}. \tag{4}$$

Here, ε_j is the dielectric constant at the position $\boldsymbol{r}_j$, $\varepsilon_0$is the dielectric constant of vacuumand d is the diameter of the dipoles. The interaction of the dipoles with themselves is given byA_{jj}, which is defined as the inverse of α_j. Left multiplication of Equation 2 with A_{jj} therefore leads to

$$A_{jj}\boldsymbol{P}_j = \boldsymbol{E}_{inc,j} - \sum_{k\neq j}^{N} A_{jk}\boldsymbol{P}_k \text{ or } \boldsymbol{E}_{inc,j} = \sum_{k=1}^{N} A_{jk}\boldsymbol{P}_k. \tag{5),(6}$$

The matrix A_{jk} of this complex linear system of equations has a block Toeplitz structure. Thus the system can efficiently be solved by the use of the fast Fourier transform (FFT). Further, the algorithm of the FFT can be parallelized and therefore the transform can be calculated by the numerous processors of a computer graphic card (GPU) [6]. Exploiting the hardware structure of the GPU accelerates the computation time compared to a CPU-calculation and thus makes the DDA admissible to solve the addressed problems.

The solution of the linear system of equations delivers the polarization vectors $\boldsymbol{P}_j$, which enables to calculate the scattered far-field according to

$$\boldsymbol{E}_{scat}(\boldsymbol{r}) = \frac{1}{4\pi\varepsilon_0}\sum_{j=1}^{N}\left\{\frac{k^2}{r}\hat{\boldsymbol{r}}\times\boldsymbol{P}_j\times\boldsymbol{r} + \left(\frac{1}{r^3} - \frac{ik}{r^2}\right)\left[3\hat{\boldsymbol{r}}(\hat{\boldsymbol{r}}\cdot\boldsymbol{P}_j) - \boldsymbol{P}_j\right]\right\}\exp(ikr). \tag{7}$$

Here,$r = |\boldsymbol{r} - \boldsymbol{r}_j|$ is the distance from the jth point dipole to the scattering field position and $\hat{\boldsymbol{r}} = \left(\boldsymbol{r} - \boldsymbol{r}_j\right)/r$ is the unit vector in the respective direction. A comprehensive portrayal of the discrete dipole approximation and the respective numerical solution procedure can be found in [7, 8, 9].

2.2 Simulated Measurement Setup

Fig. 3a shows the simulated light scattering measurement system. From above a Gaussian laser beam illuminates a nanostructured surface lying in a horizontal plane. The scattering of the light is calculated by the GPU optimized open source software ADDA [10]. For the whole discretized solid angle range the amplitude of the scattered light is computed. The result can be interpreted as the light intensity measured by a detector in an arbitrary but fixed distance from the illumination center.

As mentioned above, a finite set of dipoles approximates the scattering object. The dipoles are ordered on a regular grid to allow the application of the FFT. The distance between them has to be sufficiently small to accurately model the features of the object. In addition, at least ten dipoles per wavelength are needed for an accurate result.

Fig. 2 shows the simulated surfaces as a qualitative replica of the nanograss structures ofFig. 1. The surface on the left is defect-free, whilst the one on the right is not. The rods are statistically distributed. Defect parameters are the dimension, the density and the orientation of the rods.

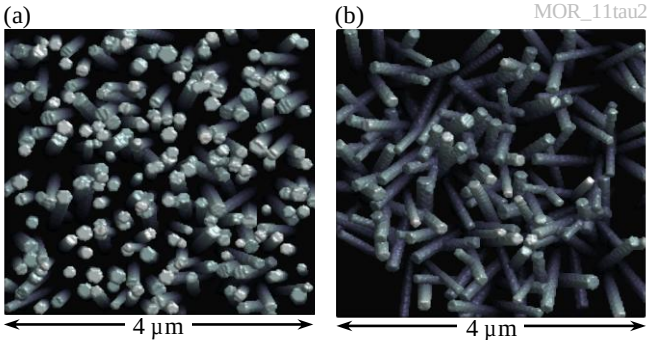

Figure 2.Computer generated model of an (a) intact nanograss

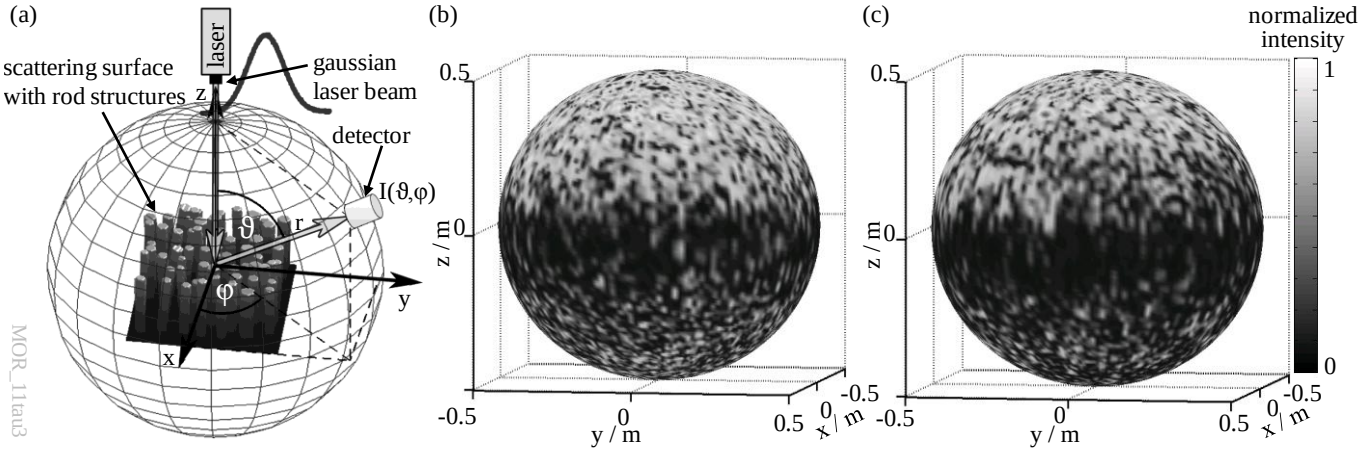

Figure 3.Simulation of the scattering fields of a nanograss structure: (a) schematic setup; (b and c) simulated logarithmic representation of the standardized scattering field intensity in arbitrary units, for scattering on a (b) defect-free and (c) defective nanostructure.

structure; (b) nanograss structure withstatistically bended rods.

The hardware limits the maximal number of dipoles to about 10^6. In order to avoid diffraction phenomena from the surface border, the laser beam diameter has to be smaller than the surface diameter. Further the beam has a Gaussian profile with a light wavelength $\lambda = 405$ nm. The refractive index is set to $\varepsilon = 1.5$ and the substrate height to h = 60 nm, thus the light is not fully reflected and partially transmits through the surface. Consequently also the scattering of this transmitted light can be calculated.

2.3 Simulation Results

Fig. 3b and 3c show in standardized arbitrary units the scattered light intensity patterns, which are calculated by the DDA. There are visible differences between the scattered light patterns. On the defect-free surface (Fig. 1a and 2a) the rods are distributed homogenously with high density. This configuration leads to widely spread light scattering pattern in the solid angles. In contrast, on the defective surface (Fig. 1b and 2b) the density of the rods is lower and there even exist blank areas without nano-rods. Hence, in comparison this object scattersless light. Consequently, the scattering pattern reveals amore sparse distribution in the solid angles.

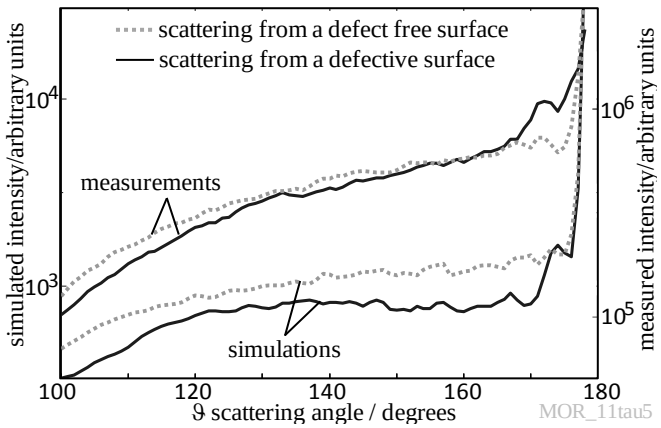

Figure 4.Intensity average over the φ-axis plotted against the ϑ-axis.

A more quantitative view of this issueis demonstrated inFig. 4. The intensities are averaged over the φ-axis and plotted against the ϑ-axis for the transmitted light, i. e. for$\vartheta \in [90°, 180°]$. The values of the simulations result from the average of over five runs with different surfaces but same defect parameters. The goal is to conveniently extract the information about the qualityof the inspected object in a production process. Therefore, intensity distribution differences are evaluated to make a conclusion in this regard. The examination of Fig. 4 reveals two characteristics. First the simulations show that for ϑ below 170° the intensity of the defect-free surface is always larger than the intensity of the defective structure. As mentioned above the reason lies in the density and the distribution of the rods. The second feature is a clear peak at $\vartheta \sim 175°$ in the defective case.

3. Measurements

3.1Measurement Setup

The aim is to measure the whole solid angle range from the light which is scattered by nanostructured surfaces. Therefore, a measurement setup was constructed according to Fig. 5a. It is based on the schematic setup according to Fig. 3a. The carriage with the detector drives on an aluminum ring (Ø = 1 m) to realize the ϑ movement.By using magnetic scale sensors as an encoder, a theoretical angular resolution below 0.001 degree can be achieved. In practice the resolution is limited by the chip diameter of the supersensitive avalanche photodiode. The rotary table enables a φ resolution of approximately 0.01 degrees. In order to guarantee sufficient intensity dynamics apart from the high voltage of the avalanchediode, the laser intensity can also be readjusted in real time. The electrical control of the individual components and the management of the measuring data are done bya *National InstrumentsCompactRIO*-Board (*cRIO-9116*)with a *Virtex-5* field programmable gate array (FPGA) and a Real-Time PowerPC controller(*cRIO-9014*) with 2 GB storage.

The ZnO samples with and without defects were kindly provided by the institute of solid state physics in Bremen (IFP).The nano-rods are grown on a glass substrate, consequently the samples are transparent and as in the simulations, some of the light is scattered in forward direction. To obtain a good comparison with the simulations, the laser beam was highly focused on the sample. Therefore, the short-focus lens blocks the backscattered light,

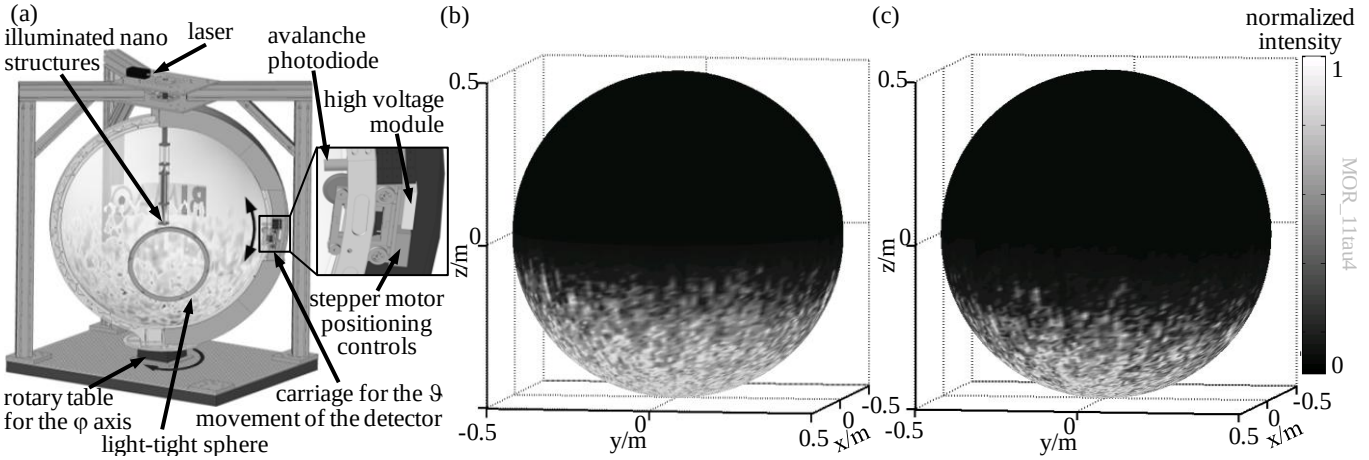

Figure 5.Measurements of the scattering fields of a nanograss structure: (a) CAD Model of the measurement setup; (b and c) measured logarithmic representation of the standardized scattering field intensity in arbitrary units, measured on a (b) defect-free and (c) defective nanostructure surface.

whereby this region cannot be measured and the upper range in Fig. 5b and 5c appears dark.

3.2 Measurement Results

The measured scattered light in forward direction is represented in Fig. 5b and 5c. Compared to the simulations, qualitatively similar measurement results occur. Again in the defect-free case the homogenous and with high density distributed rods lead to a wider expanded scattering pattern. For the measurements in both cases, the speckle size seems to be smaller than in the simulations. This effect results from differences in the incident field. In the measurement, the focused beam diameter is approximately at least 10 µm. Limited by the computation effort, this size parameter can only be set to 2 µm in the simulations. The size of the speckles in the scattered light pattern scales inversely proportional to the beam diameter. Thus the speckles in the simulations are larger.

The scattered light intensities averaged over φ, which are shown in Fig. 4, lead to the following conclusions. The differences of the intensities for ϑ below 170° are not as distinctive in the measurements as in the simulations. Over a large ϑ range the values are close to each other. Just for ϑ smaller than approximately 130° the intensities diverge. The second characteristic is the intensity peak at ϑ ~ 175° in the defective case. This feature can be recognized in the measurements and in the simulations. Accordingly the evaluation of the intensity of the scattered light in a small area around ϑ = 175° is sufficient to judge the quality of the nanostructured surface.

4. Conclusions

In this paper the hardware accelerated rigorous simulation algorithms of the DDA are qualitatively verified by a supersensitive measurement setup for the detection of angle resolved scattered light. For ZnOnanograss structures it is shown that by comparison between a multitude of simulations and measurementsone can distinguish between defect-free and defective nanograss.

For an in-process surface characterization the presented laboratory measurement setup is not applicable. The investigations show that the ϑ ~ 175° regime of the scattered light indicates the quality of a ZnOnanograsssurface. For transparent samples a simple setup using a camera positioned directly below the sample can measure the light intensities. In future work it has to be investigated whether such a setup is able to analyze the surface quality during the running growth process of the nanograss.

ACKNOWLEDGEMENT

The authors gratefully acknowledge the support provided by the German Research Foundation (DFG) within the framework of the Priority Program 1327 and the Individual Grants Program(GO 554/27-1).

REFERENCES

1. Lonardo, P.M., Bruzzone, A.A., Gambaro, C., 1991, Surface Characterization and Defect Detection by Analysis of Images Obtained with Coherent Light, Annals of the CIRP, 40/1:541-544.
2. Patzelt, S., Flucke, C., Tausendfreund, A., Goch, G., Brinksmeier, E., 2008, In-Process Characterization of Diamond Cut Prismatic Microcavities, Proc. of 10th Int. Conf. of the euspen, 2:354-357.
3. Ogilvy, J.A., 1991, Theory of Wave Scattering from Random Rough Surfaces, Bristol, Hilger.
4. Draine, B.T., 1988, The Discrete-Dipole Approximation and its Application to Interstellar Graphite Grains, The Astrophysical Journal, 333:848-872.
5. Doicu, A., Wriedt, T., Eremin, Y.A., 2006, Light Scattering by Systems of Particles, Springer, Heidelberg.
6. Kieß, S., 2010, GPU-basierte Beschleunigungder diskretenDipol-Approximation fürStreulichtsimulationen, Diploma Thesis, University of Stuttgart.
7. Shimura, K., Milster, T.D., 2001, Vector Diffraction by Discrete Dipole Approximation, Optical Society of America, 18/11:2895-2900.
8. Flatau, P.J., 2004, Fast Solvers for One Dimensional Light Scattering in the Discrete Dipole Approximation, Optics Express, 12/14:3149-3155.
9. Barrowes, B.E., Teixeira, F.L., Kong, J.A., 2001, Fast Algorithm for Matrix-Vector Multiply of Asymmetric Multilevel Block-Toeplitz Matrices in 3-D Scattering, Microwave and Optical Technology Letters, 31/1:28-32.
10. Yurkin, M.A., Maltsev, V.P., Hoekstra, A.G., 2007, The Discrete

Dipole Approximation for Simulation of Light Scattering by Particles Much Larger Than the Wavelength, J. Quant. Spectrosc. Radiat. Transfer, 106:546-557.